



HAL
open science

First observations of $\bar{B}_{s^0} \rightarrow D^+ D^-$, $D_{s^+} D^-$ and $D^0 \bar{D}^0$ decays

R. Aaij, Y. Amhis, S. Barsuk, O. Callot, J. He, O. Kochebina, J. Lefrançois,
F. Machefert, A. Martin Sanchez, M. Nicol, et al.

► To cite this version:

R. Aaij, Y. Amhis, S. Barsuk, O. Callot, J. He, et al.. First observations of $\bar{B}_{s^0} \rightarrow D^+ D^-$, $D_{s^+} D^-$ and $D^0 \bar{D}^0$ decays. Physical Review D, 2013, 87, pp.092007. 10.1103/PhysRevD.87.092007. in2p3-00794581

HAL Id: in2p3-00794581

<https://hal.in2p3.fr/in2p3-00794581>

Submitted on 4 Sep 2023

HAL is a multi-disciplinary open access archive for the deposit and dissemination of scientific research documents, whether they are published or not. The documents may come from teaching and research institutions in France or abroad, or from public or private research centers.

L'archive ouverte pluridisciplinaire **HAL**, est destinée au dépôt et à la diffusion de documents scientifiques de niveau recherche, publiés ou non, émanant des établissements d'enseignement et de recherche français ou étrangers, des laboratoires publics ou privés.



First observations of $\bar{B}_s^0 \rightarrow D^+ D^-$, $D_s^+ D^-$ and $D^0 \bar{D}^0$ decays

The LHCb collaboration[†]

Abstract

First observations and measurements of the branching fractions of the $\bar{B}_s^0 \rightarrow D^+ D^-$, $\bar{B}_s^0 \rightarrow D_s^+ D^-$ and $\bar{B}_s^0 \rightarrow D^0 \bar{D}^0$ decays are presented using 1.0 fb^{-1} of data collected by the LHCb experiment. These branching fractions are normalized to those of $\bar{B}^0 \rightarrow D^+ D^-$, $B^0 \rightarrow D_s^+ D^-$ and $B^- \rightarrow D^0 D_s^-$, respectively. An excess of events consistent with the decay $\bar{B}^0 \rightarrow D^0 \bar{D}^0$ is also seen, and its branching fraction is measured relative to that of $B^- \rightarrow D^0 D_s^-$. Improved measurements of the branching fractions $\mathcal{B}(\bar{B}_s^0 \rightarrow D_s^+ D^-)$ and $\mathcal{B}(B^- \rightarrow D^0 D_s^-)$ are reported, each relative to $\mathcal{B}(B^0 \rightarrow D_s^+ D^-)$. The ratios of branching fractions are

$$\begin{aligned} \frac{\mathcal{B}(\bar{B}_s^0 \rightarrow D^+ D^-)}{\mathcal{B}(\bar{B}^0 \rightarrow D^+ D^-)} &= 1.08 \pm 0.20 \pm 0.10, \\ \frac{\mathcal{B}(\bar{B}_s^0 \rightarrow D_s^+ D^-)}{\mathcal{B}(B^0 \rightarrow D_s^+ D^-)} &= 0.050 \pm 0.008 \pm 0.004, \\ \frac{\mathcal{B}(\bar{B}_s^0 \rightarrow D^0 \bar{D}^0)}{\mathcal{B}(B^- \rightarrow D^0 D_s^-)} &= 0.019 \pm 0.003 \pm 0.003, \\ \frac{\mathcal{B}(\bar{B}^0 \rightarrow D^0 \bar{D}^0)}{\mathcal{B}(B^- \rightarrow D^0 D_s^-)} &= 0.0014 \pm 0.0006 \pm 0.0002, \\ \frac{\mathcal{B}(\bar{B}_s^0 \rightarrow D_s^+ D_s^-)}{\mathcal{B}(B^0 \rightarrow D_s^+ D^-)} &= 0.56 \pm 0.03 \pm 0.04, \\ \frac{\mathcal{B}(B^- \rightarrow D^0 D_s^-)}{\mathcal{B}(B^0 \rightarrow D_s^+ D^-)} &= 1.22 \pm 0.02 \pm 0.07, \end{aligned}$$

where the uncertainties are statistical and systematic, respectively.

Submitted to Physical Review D

© CERN on behalf of the LHCb collaboration, license CC-BY-3.0.

[†]Authors are listed on the following pages.

LHCb collaboration

R. Aaij⁴⁰, C. Abellan Beteta^{35,n}, B. Adeva³⁶, M. Adinolfi⁴⁵, C. Adrover⁶, A. Affolder⁵¹, Z. Ajaltouni⁵, J. Albrecht⁹, F. Alessio³⁷, M. Alexander⁵⁰, S. Ali⁴⁰, G. Alkhazov²⁹, P. Alvarez Cartelle³⁶, A.A. Alves Jr^{24,37}, S. Amato², S. Amerio²¹, Y. Amhis⁷, L. Anderlini^{17,f}, J. Anderson³⁹, R. Andreassen⁵⁹, R.B. Appleby⁵³, O. Aquines Gutierrez¹⁰, F. Archilli¹⁸, A. Artamonov³⁴, M. Artuso⁵⁶, E. Aslanides⁶, G. Auriemma^{24,m}, S. Bachmann¹¹, J.J. Back⁴⁷, C. Baesso⁵⁷, V. Balagura³⁰, W. Baldini¹⁶, R.J. Barlow⁵³, C. Barschel³⁷, S. Barsuk⁷, W. Barter⁴⁶, Th. Bauer⁴⁰, A. Bay³⁸, J. Beddow⁵⁰, F. Bedeschi²², I. Bediaga¹, S. Belogurov³⁰, K. Belous³⁴, I. Belyaev³⁰, E. Ben-Haim⁸, M. Benayoun⁸, G. Bencivenni¹⁸, S. Benson⁴⁹, J. Benton⁴⁵, A. Berezhtoy³¹, R. Bernet³⁹, M.-O. Bettler⁴⁶, M. van Beuzekom⁴⁰, A. Bien¹¹, S. Bifani¹², T. Bird⁵³, A. Bizzeti^{17,h}, P.M. Bjørnstad⁵³, T. Blake³⁷, F. Blanc³⁸, J. Blouw¹¹, S. Blusk⁵⁶, V. Bocci²⁴, A. Bondar³³, N. Bondar²⁹, W. Bonivento¹⁵, S. Borghi⁵³, A. Borgia⁵⁶, T.J.V. Bowcock⁵¹, E. Bowen³⁹, C. Bozzi¹⁶, T. Brambach⁹, J. van den Brand⁴¹, J. Bressieux³⁸, D. Brett⁵³, M. Britsch¹⁰, T. Britton⁵⁶, N.H. Brook⁴⁵, H. Brown⁵¹, I. Burducea²⁸, A. Bursche³⁹, G. Busetto^{21,q}, J. Buytaert³⁷, S. Cadeddu¹⁵, O. Callot⁷, M. Calvi^{20,j}, M. Calvo Gomez^{35,n}, A. Camboni³⁵, P. Campana^{18,37}, A. Carbone^{14,c}, G. Carboni^{23,k}, R. Cardinale^{19,i}, A. Cardini¹⁵, H. Carranza-Mejia⁴⁹, L. Carson⁵², K. Carvalho Akiba², G. Casse⁵¹, M. Cattaneo³⁷, Ch. Cauet⁹, M. Charles⁵⁴, Ph. Charpentier³⁷, P. Chen^{3,38}, N. Chiapolini³⁹, M. Chrzaszcz²⁵, K. Ciba³⁷, X. Cid Vidal³⁶, G. Ciezarek⁵², P.E.L. Clarke⁴⁹, M. Clemencic³⁷, H.V. Cliff⁴⁶, J. Closier³⁷, C. Coca²⁸, V. Coco⁴⁰, J. Cogan⁶, E. Cogneras⁵, P. Collins³⁷, A. Comerma-Montells³⁵, A. Contu¹⁵, A. Cook⁴⁵, M. Coombes⁴⁵, S. Coquereau⁸, G. Corti³⁷, B. Couturier³⁷, G.A. Cowan³⁸, D. Craik⁴⁷, S. Cunliffe⁵², R. Currie⁴⁹, C. D'Ambrosio³⁷, P. David⁸, P.N.Y. David⁴⁰, I. De Bonis⁴, K. De Bruyn⁴⁰, S. De Capua⁵³, M. De Cian³⁹, J.M. De Miranda¹, M. De Oyanguren Campos^{35,o}, L. De Paula², W. De Silva⁵⁹, P. De Simone¹⁸, D. Decamp⁴, M. Deckenhoff⁹, L. Del Buono⁸, D. Derkach¹⁴, O. Deschamps⁵, F. Dettori⁴¹, A. Di Canto¹¹, H. Dijkstra³⁷, M. Dogaru²⁸, S. Donleavy⁵¹, F. Dordei¹¹, A. Dosil Suárez³⁶, D. Dossett⁴⁷, A. Dovbnya⁴², F. Dupertuis³⁸, R. Dzhelyadin³⁴, A. Dziurda²⁵, A. Dzyuba²⁹, S. Easo^{48,37}, U. Egede⁵², V. Egorychev³⁰, S. Eidelman³³, D. van Eijk⁴⁰, S. Eisenhardt⁴⁹, U. Eitschberger⁹, R. Ekelhof⁹, L. Eklund⁵⁰, I. El Rifai⁵, Ch. Elsasser³⁹, D. Elsby⁴⁴, A. Falabella^{14,e}, C. Färber¹¹, G. Fardell⁴⁹, C. Farinelli⁴⁰, S. Farry¹², V. Fave³⁸, D. Ferguson⁴⁹, V. Fernandez Albor³⁶, F. Ferreira Rodrigues¹, M. Ferro-Luzzi³⁷, S. Filippov³², C. Fitzpatrick³⁷, M. Fontana¹⁰, F. Fontanelli^{19,i}, R. Forty³⁷, O. Francisco², M. Frank³⁷, C. Frei³⁷, M. Frosini^{17,f}, S. Furcas²⁰, E. Furfaro²³, A. Gallas Torreira³⁶, D. Galli^{14,c}, M. Gandelman², P. Gandini⁵⁴, Y. Gao³, J. Garofoli⁵⁶, P. Garosi⁵³, J. Garra Tico⁴⁶, L. Garrido³⁵, C. Gaspar³⁷, R. Gauld⁵⁴, E. Gersabeck¹¹, M. Gersabeck⁵³, T. Gershon^{47,37}, Ph. Ghez⁴, V. Gibson⁴⁶, V.V. Gligorov³⁷, C. Göbel⁵⁷, D. Golubkov³⁰, A. Golutvin^{52,30,37}, A. Gomes², H. Gordon⁵⁴, M. Grabalosa Gándara⁵, R. Graciani Diaz³⁵, L.A. Granado Cardoso³⁷, E. Graugés³⁵, G. Graziani¹⁷, A. Grecu²⁸, E. Greening⁵⁴, S. Gregson⁴⁶, O. Grünberg⁵⁸, B. Gui⁵⁶, E. Gushchin³², Yu. Guz³⁴, T. Gys³⁷, C. Hadjivasiliou⁵⁶, G. Haefeli³⁸, C. Haen³⁷, S.C. Haines⁴⁶, S. Hall⁵², T. Hampson⁴⁵, S. Hansmann-Menzemer¹¹, N. Harnew⁵⁴, S.T. Harnew⁴⁵, J. Harrison⁵³, T. Hartmann⁵⁸, J. He⁷, V. Heijne⁴⁰, K. Hennessy⁵¹, P. Henrard⁵, J.A. Hernando Morata³⁶, E. van Herwijnen³⁷, E. Hicks⁵¹, D. Hill⁵⁴, M. Hoballah⁵, C. Hombach⁵³, P. Hopchev⁴, W. Hulsbergen⁴⁰, P. Hunt⁵⁴, T. Huse⁵¹, N. Hussain⁵⁴, D. Hutchcroft⁵¹, D. Hynds⁵⁰, V. Iakovenko⁴³, M. Idzik²⁶, P. Ilten¹², R. Jacobsson³⁷, A. Jaeger¹¹, E. Jans⁴⁰, P. Jaton³⁸, F. Jing³, M. John⁵⁴, D. Johnson⁵⁴, C.R. Jones⁴⁶, B. Jost³⁷, M. Kabbalo⁹, S. Kandybei⁴²,

M. Karacson³⁷, T.M. Karbach³⁷, I.R. Kenyon⁴⁴, U. Kerzel³⁷, T. Ketel⁴¹, A. Keune³⁸,
B. Khanji²⁰, O. Kochebina⁷, I. Komarov^{38,31}, R.F. Koopman⁴¹, P. Koppenburg⁴⁰, M. Korolev³¹,
A. Kozlinskiy⁴⁰, L. Kravchuk³², K. Kreplin¹¹, M. Kreps⁴⁷, G. Krocker¹¹, P. Krovovny³³,
F. Kruse⁹, M. Kucharczyk^{20,25,j}, V. Kudryavtsev³³, T. Kvaratskheliya^{30,37}, V.N. La Thi³⁸,
D. Lacarrere³⁷, G. Lafferty⁵³, A. Lai¹⁵, D. Lambert⁴⁹, R.W. Lambert⁴¹, E. Lanciotti³⁷,
G. Lanfranchi^{18,37}, C. Langenbruch³⁷, T. Latham⁴⁷, C. Lazzeroni⁴⁴, R. Le Gac⁶,
J. van Leerdam⁴⁰, J.-P. Lees⁴, R. Lefèvre⁵, A. Leflat^{31,37}, J. Lefrançois⁷, S. Leo²², O. Leroy⁶,
B. Leverington¹¹, Y. Li³, L. Li Gioi⁵, M. Liles⁵¹, R. Lindner³⁷, C. Linn¹¹, B. Liu³, G. Liu³⁷,
J. von Loeben²⁰, S. Lohn³⁷, J.H. Lopes², E. Lopez Asamar³⁵, N. Lopez-March³⁸, H. Lu³,
D. Lucchesi^{21,q}, J. Luisier³⁸, H. Luo⁴⁹, F. Machefert⁷, I.V. Machikhiliyan^{4,30}, F. Maciuc²⁸,
O. Maev^{29,37}, S. Malde⁵⁴, G. Manca^{15,d}, G. Mancinelli⁶, U. Marconi¹⁴, R. Märki³⁸, J. Marks¹¹,
G. Martellotti²⁴, A. Martens⁸, L. Martin⁵⁴, A. Martín Sánchez⁷, M. Martinelli⁴⁰,
D. Martinez Santos⁴¹, D. Martins Tostes², A. Massafferri¹, R. Matev³⁷, Z. Mathe³⁷,
C. Matteuzzi²⁰, E. Maurice⁶, A. Mazurov^{16,32,37,e}, J. McCarthy⁴⁴, R. McNulty¹², A. McNab⁵³,
B. Meadows^{59,54}, F. Meier⁹, M. Meissner¹¹, M. Merk⁴⁰, D.A. Milanes⁸, M.-N. Minard⁴,
J. Molina Rodriguez⁵⁷, S. Monteil⁵, D. Moran⁵³, P. Morawski²⁵, M.J. Morello^{22,s},
R. Mountain⁵⁶, I. Mous⁴⁰, F. Muheim⁴⁹, K. Müller³⁹, R. Muresan²⁸, B. Muryn²⁶, B. Muster³⁸,
P. Naik⁴⁵, T. Nakada³⁸, R. Nandakumar⁴⁸, I. Nasteva¹, M. Needham⁴⁹, N. Neufeld³⁷,
A.D. Nguyen³⁸, T.D. Nguyen³⁸, C. Nguyen-Mau^{38,p}, M. Nicol⁷, V. Niess⁵, R. Niet⁹, N. Nikitin³¹,
T. Nikodem¹¹, A. Nomerotski⁵⁴, A. Novoselov³⁴, A. Oblakowska-Mucha²⁶, V. Obraztsov³⁴,
S. Oggero⁴⁰, S. Ogilvy⁵⁰, O. Okhrimenko⁴³, R. Oldeman^{15,d,37}, M. Orlandea²⁸,
J.M. Otalora Goicochea², P. Owen⁵², B.K. Pal⁵⁶, A. Palano^{13,b}, M. Palutan¹⁸, J. Panman³⁷,
A. Papanestis⁴⁸, M. Pappagallo⁵⁰, C. Parkes⁵³, C.J. Parkinson⁵², G. Passaleva¹⁷, G.D. Patel⁵¹,
M. Patel⁵², G.N. Patrick⁴⁸, C. Patrignani^{19,i}, C. Pavel-Nicorescu²⁸, A. Pazos Alvarez³⁶,
A. Pellegrino⁴⁰, G. Penso^{24,l}, M. Pepe Altarelli³⁷, S. Perazzini^{14,c}, D.L. Perego^{20,j},
E. Perez Trigo³⁶, A. Pérez-Calero Yzquierdo³⁵, P. Perret⁵, M. Perrin-Terrin⁶, G. Pessina²⁰,
K. Petridis⁵², A. Petrolini^{19,i}, A. Phan⁵⁶, E. Picatoste Olloqui³⁵, B. Pietrzyk⁴, T. Pilar⁴⁷,
D. Pinci²⁴, S. Playfer⁴⁹, M. Plo Casasus³⁶, F. Polci⁸, G. Polok²⁵, A. Poluektov^{47,33},
E. Polcarpo², D. Popov¹⁰, B. Popovici²⁸, C. Potterat³⁵, A. Powell⁵⁴, J. Prisciandaro³⁸,
V. Pugatch⁴³, A. Puig Navarro³⁸, G. Punzi^{22,r}, W. Qian⁴, J.H. Rademacker⁴⁵,
B. Rakotomiamanana³⁸, M.S. Rangel², I. Raniuk⁴², N. Rauschmayr³⁷, G. Raven⁴¹,
S. Redford⁵⁴, M.M. Reid⁴⁷, A.C. dos Reis¹, S. Ricciardi⁴⁸, A. Richards⁵², K. Rinnert⁵¹,
V. Rives Molina³⁵, D.A. Roa Romero⁵, P. Robbe⁷, E. Rodrigues⁵³, P. Rodriguez Perez³⁶,
S. Roiser³⁷, V. Romanovsky³⁴, A. Romero Vidal³⁶, J. Rouvinet³⁸, T. Ruf³⁷, F. Ruffini²²,
H. Ruiz³⁵, P. Ruiz Valls^{35,o}, G. Sabatino^{24,k}, J.J. Saborido Silva³⁶, N. Sagidova²⁹, P. Sail⁵⁰,
B. Saitta^{15,d}, C. Salzmann³⁹, B. Sanmartin Sedes³⁶, M. Sannino^{19,i}, R. Santacesaria²⁴,
C. Santamarina Rios³⁶, E. Santovetti^{23,k}, M. Sapunov⁶, A. Sarti^{18,l}, C. Satriano^{24,m}, A. Satta²³,
M. Savrie^{16,e}, D. Savrina^{30,31}, P. Schaack⁵², M. Schiller⁴¹, H. Schindler³⁷, M. Schlupp⁹,
M. Schmelling¹⁰, B. Schmidt³⁷, O. Schneider³⁸, A. Schopper³⁷, M.-H. Schune⁷, R. Schwemmer³⁷,
B. Sciascia¹⁸, A. Sciubba²⁴, M. Seco³⁶, A. Semennikov³⁰, K. Senderowska²⁶, I. Sepp⁵²,
N. Serra³⁹, J. Serrano⁶, P. Seyfert¹¹, M. Shapkin³⁴, I. Shapoval^{42,37}, P. Shatalov³⁰,
Y. Shcheglov²⁹, T. Shears^{51,37}, L. Shekhtman³³, O. Shevchenko⁴², V. Shevchenko³⁰, A. Shires⁵²,
R. Silva Coutinho⁴⁷, T. Skwarnicki⁵⁶, N.A. Smith⁵¹, E. Smith^{54,48}, M. Smith⁵³, M.D. Sokoloff⁵⁹,
F.J.P. Soler⁵⁰, F. Soomro^{18,37}, D. Souza⁴⁵, B. Souza De Paula², B. Spaan⁹, A. Sparkes⁴⁹,
P. Spradlin⁵⁰, F. Stagni³⁷, S. Stahl¹¹, O. Steinkamp³⁹, S. Stoica²⁸, S. Stone⁵⁶, B. Storaci³⁹,
M. Straticiu²⁸, U. Straumann³⁹, V.K. Subbiah³⁷, S. Swientek⁹, V. Syropoulos⁴¹,

M. Szczekowski²⁷, P. Szczypka^{38,37}, T. Szumlak²⁶, S. T’Jampens⁴, M. Teklishyn⁷,
E. Teodorescu²⁸, F. Teubert³⁷, C. Thomas⁵⁴, E. Thomas³⁷, J. van Tilburg¹¹, V. Tisserand⁴,
M. Tobin³⁹, S. Tolk⁴¹, D. Tonelli³⁷, S. Topp-Joergensen⁵⁴, N. Torr⁵⁴, E. Tournefier^{4,52},
S. Tourneur³⁸, M.T. Tran³⁸, M. Tresch³⁹, A. Tsaregorodtsev⁶, P. Tsopelas⁴⁰, N. Tuning⁴⁰,
M. Ubeda Garcia³⁷, A. Ukleja²⁷, D. Urner⁵³, U. Uwer¹¹, V. Vagnoni¹⁴, G. Valenti¹⁴,
R. Vazquez Gomez³⁵, P. Vazquez Regueiro³⁶, S. Vecchi¹⁶, J.J. Velthuis⁴⁵, M. Veltri^{17,g},
G. Veneziano³⁸, M. Vesterinen³⁷, B. Viaud⁷, D. Vieira², X. Vilasis-Cardona^{35,n}, A. Vollhardt³⁹,
D. Volyanskyy¹⁰, D. Voong⁴⁵, A. Vorobyev²⁹, V. Vorobyev³³, C. Voß⁵⁸, H. Voss¹⁰, R. Waldi⁵⁸,
R. Wallace¹², S. Wandernoth¹¹, J. Wang⁵⁶, D.R. Ward⁴⁶, N.K. Watson⁴⁴, A.D. Webber⁵³,
D. Websdale⁵², M. Whitehead⁴⁷, J. Wicht³⁷, J. Wiechczynski²⁵, D. Wiedner¹¹, L. Wiggers⁴⁰,
G. Wilkinson⁵⁴, M.P. Williams^{47,48}, M. Williams⁵⁵, F.F. Wilson⁴⁸, J. Wishahi⁹, M. Witek²⁵,
S.A. Wotton⁴⁶, S. Wright⁴⁶, S. Wu³, K. Wyllie³⁷, Y. Xie^{49,37}, F. Xing⁵⁴, Z. Xing⁵⁶, Z. Yang³,
R. Young⁴⁹, X. Yuan³, O. Yushchenko³⁴, M. Zangoli¹⁴, M. Zavertyaev^{10,a}, F. Zhang³,
L. Zhang⁵⁶, W.C. Zhang¹², Y. Zhang³, A. Zhelezov¹¹, A. Zhokhov³⁰, L. Zhong³, A. Zvyagin³⁷.

¹ *Centro Brasileiro de Pesquisas Físicas (CBPF), Rio de Janeiro, Brazil*

² *Universidade Federal do Rio de Janeiro (UFRJ), Rio de Janeiro, Brazil*

³ *Center for High Energy Physics, Tsinghua University, Beijing, China*

⁴ *LAPP, Université de Savoie, CNRS/IN2P3, Annecy-Le-Vieux, France*

⁵ *Clermont Université, Université Blaise Pascal, CNRS/IN2P3, LPC, Clermont-Ferrand, France*

⁶ *CPPM, Aix-Marseille Université, CNRS/IN2P3, Marseille, France*

⁷ *LAL, Université Paris-Sud, CNRS/IN2P3, Orsay, France*

⁸ *LPNHE, Université Pierre et Marie Curie, Université Paris Diderot, CNRS/IN2P3, Paris, France*

⁹ *Fakultät Physik, Technische Universität Dortmund, Dortmund, Germany*

¹⁰ *Max-Planck-Institut für Kernphysik (MPIK), Heidelberg, Germany*

¹¹ *Physikalisches Institut, Ruprecht-Karls-Universität Heidelberg, Heidelberg, Germany*

¹² *School of Physics, University College Dublin, Dublin, Ireland*

¹³ *Sezione INFN di Bari, Bari, Italy*

¹⁴ *Sezione INFN di Bologna, Bologna, Italy*

¹⁵ *Sezione INFN di Cagliari, Cagliari, Italy*

¹⁶ *Sezione INFN di Ferrara, Ferrara, Italy*

¹⁷ *Sezione INFN di Firenze, Firenze, Italy*

¹⁸ *Laboratori Nazionali dell’INFN di Frascati, Frascati, Italy*

¹⁹ *Sezione INFN di Genova, Genova, Italy*

²⁰ *Sezione INFN di Milano Bicocca, Milano, Italy*

²¹ *Sezione INFN di Padova, Padova, Italy*

²² *Sezione INFN di Pisa, Pisa, Italy*

²³ *Sezione INFN di Roma Tor Vergata, Roma, Italy*

²⁴ *Sezione INFN di Roma La Sapienza, Roma, Italy*

²⁵ *Henryk Niewodniczanski Institute of Nuclear Physics Polish Academy of Sciences, Kraków, Poland*

²⁶ *AGH University of Science and Technology, Kraków, Poland*

²⁷ *National Center for Nuclear Research (NCBJ), Warsaw, Poland*

²⁸ *Horia Hulubei National Institute of Physics and Nuclear Engineering, Bucharest-Magurele, Romania*

²⁹ *Petersburg Nuclear Physics Institute (PNPI), Gatchina, Russia*

³⁰ *Institute of Theoretical and Experimental Physics (ITEP), Moscow, Russia*

³¹ *Institute of Nuclear Physics, Moscow State University (SINP MSU), Moscow, Russia*

³² *Institute for Nuclear Research of the Russian Academy of Sciences (INR RAN), Moscow, Russia*

³³ *Budker Institute of Nuclear Physics (SB RAS) and Novosibirsk State University, Novosibirsk, Russia*

³⁴ *Institute for High Energy Physics (IHEP), Protvino, Russia*

³⁵ *Universitat de Barcelona, Barcelona, Spain*

- ³⁶ *Universidad de Santiago de Compostela, Santiago de Compostela, Spain*
- ³⁷ *European Organization for Nuclear Research (CERN), Geneva, Switzerland*
- ³⁸ *Ecole Polytechnique Fédérale de Lausanne (EPFL), Lausanne, Switzerland*
- ³⁹ *Physik-Institut, Universität Zürich, Zürich, Switzerland*
- ⁴⁰ *Nikhef National Institute for Subatomic Physics, Amsterdam, The Netherlands*
- ⁴¹ *Nikhef National Institute for Subatomic Physics and VU University Amsterdam, Amsterdam, The Netherlands*
- ⁴² *NSC Kharkiv Institute of Physics and Technology (NSC KIPT), Kharkiv, Ukraine*
- ⁴³ *Institute for Nuclear Research of the National Academy of Sciences (KINR), Kyiv, Ukraine*
- ⁴⁴ *University of Birmingham, Birmingham, United Kingdom*
- ⁴⁵ *H.H. Wills Physics Laboratory, University of Bristol, Bristol, United Kingdom*
- ⁴⁶ *Cavendish Laboratory, University of Cambridge, Cambridge, United Kingdom*
- ⁴⁷ *Department of Physics, University of Warwick, Coventry, United Kingdom*
- ⁴⁸ *STFC Rutherford Appleton Laboratory, Didcot, United Kingdom*
- ⁴⁹ *School of Physics and Astronomy, University of Edinburgh, Edinburgh, United Kingdom*
- ⁵⁰ *School of Physics and Astronomy, University of Glasgow, Glasgow, United Kingdom*
- ⁵¹ *Oliver Lodge Laboratory, University of Liverpool, Liverpool, United Kingdom*
- ⁵² *Imperial College London, London, United Kingdom*
- ⁵³ *School of Physics and Astronomy, University of Manchester, Manchester, United Kingdom*
- ⁵⁴ *Department of Physics, University of Oxford, Oxford, United Kingdom*
- ⁵⁵ *Massachusetts Institute of Technology, Cambridge, MA, United States*
- ⁵⁶ *Syracuse University, Syracuse, NY, United States*
- ⁵⁷ *Pontificia Universidade Católica do Rio de Janeiro (PUC-Rio), Rio de Janeiro, Brazil, associated to ²*
- ⁵⁸ *Institut für Physik, Universität Rostock, Rostock, Germany, associated to ¹¹*
- ⁵⁹ *University of Cincinnati, Cincinnati, OH, United States, associated to ⁵⁶*

^a *P.N. Lebedev Physical Institute, Russian Academy of Science (LPI RAS), Moscow, Russia*

^b *Università di Bari, Bari, Italy*

^c *Università di Bologna, Bologna, Italy*

^d *Università di Cagliari, Cagliari, Italy*

^e *Università di Ferrara, Ferrara, Italy*

^f *Università di Firenze, Firenze, Italy*

^g *Università di Urbino, Urbino, Italy*

^h *Università di Modena e Reggio Emilia, Modena, Italy*

ⁱ *Università di Genova, Genova, Italy*

^j *Università di Milano Bicocca, Milano, Italy*

^k *Università di Roma Tor Vergata, Roma, Italy*

^l *Università di Roma La Sapienza, Roma, Italy*

^m *Università della Basilicata, Potenza, Italy*

ⁿ *LIFAELS, La Salle, Universitat Ramon Llull, Barcelona, Spain*

^o *IFIC, Universitat de Valencia-CSIC, Valencia, Spain*

^p *Hanoi University of Science, Hanoi, Viet Nam*

^q *Università di Padova, Padova, Italy*

^r *Università di Pisa, Pisa, Italy*

^s *Scuola Normale Superiore, Pisa, Italy*

1 Introduction

Double-charm decays of B mesons can be used to probe the Cabibbo-Kobayashi-Maskawa matrix [1, 2] elements, and provide a laboratory to study final state interactions. The time-dependent CP asymmetry in the $B^0 \rightarrow D^+ D^-$ decay provides a way to measure the B^0 mixing phase [3, 4], where information from other double-charm final states can be used to account for loop (penguin) contributions and other non-factorizable effects [5–9]. Double-charm decays of B mesons can also be used to measure the weak phase γ , assuming U -spin symmetry [10, 11]. The purely CP -even $\bar{B}_s^0 \rightarrow D_s^+ D_s^-$ decay is also of interest, as it can be used to measure the B_s^0 mixing phase. Moreover, a lifetime measurement using the $\bar{B}_s^0 \rightarrow D_s^+ D_s^-$ decay provides complementary information on $\Delta\Gamma_s$ [11–13] to that obtained from direct measurements [14], or from lifetime measurements in other CP eigenstates [15, 16].

The study of $B \rightarrow D\bar{D}'$ decays¹ can also provide a better theoretical understanding of the processes that contribute to B meson decay. Feynman diagrams contributing to the decays considered in this paper are shown in Fig. 1. The $\bar{B}_s^0 \rightarrow D^0 \bar{D}^0$, $\bar{B}_s^0 \rightarrow D^+ D^-$ and $\bar{B}^0 \rightarrow D^0 \bar{D}^0$ decays are mediated by the W -exchange amplitude, along with penguin-annihilation contributions and rescattering [17]. The only other observed B meson decays of this type are $\bar{B}^0 \rightarrow D_s^{(*)+} K^{(*)-}$ and $\bar{B}_s^0 \rightarrow \pi^+ \pi^-$, with branching fractions of the order of 10^{-5} [18] and 10^{-6} [19], respectively. Predictions of the $\bar{B}_s^0 \rightarrow D^+ D^-$ branching fraction using perturbative approaches yield 3.6×10^{-3} [20], while the use of non-perturbative approaches has led to a smaller value of 1×10^{-3} [21]. More recent phenomenological studies, which assume a dominant contribution from rescattering, predict a significantly lower branching fraction of $\mathcal{B}(\bar{B}_s^0 \rightarrow D^+ D^-) = \mathcal{B}(\bar{B}_s^0 \rightarrow D^0 \bar{D}^0) = (7.8 \pm 4.7) \times 10^{-5}$ [17].

This paper reports the first observations of the $\bar{B}_s^0 \rightarrow D^+ D^-$, $\bar{B}_s^0 \rightarrow D_s^+ D^-$ and $\bar{B}_s^0 \rightarrow D^0 \bar{D}^0$ decays, and measurements of their branching fractions normalized relative to those of $\bar{B}^0 \rightarrow D^+ D^-$, $B^0 \rightarrow D_s^+ D^-$ and $B^- \rightarrow D^0 D_s^-$, respectively. An excess of events consistent with $\bar{B}^0 \rightarrow D^0 \bar{D}^0$ is also seen, and its branching fraction is reported. Improved measurements of the ratios of branching fractions $\mathcal{B}(\bar{B}_s^0 \rightarrow D_s^+ D_s^-)/\mathcal{B}(B^0 \rightarrow D_s^+ D^-)$ and $\mathcal{B}(B^- \rightarrow D^0 D_s^-)/\mathcal{B}(B^0 \rightarrow D_s^+ D^-)$ are also presented. All results are based upon an integrated luminosity of 1.0 fb^{-1} of pp collision data at $\sqrt{s} = 7 \text{ TeV}$ recorded by the LHCb experiment in 2011. Inclusion of charge conjugate final states is implied throughout.

2 Data sample and candidate selection

The LHCb detector [22] is a single-arm forward spectrometer covering the pseudorapidity range $2 < \eta < 5$, designed for the study of particles containing b or c quarks. The detector includes a high precision tracking system consisting of a silicon-strip vertex detector surrounding the pp interaction region, a large-area silicon-strip detector located upstream of a dipole magnet with a bending power of about 4 Tm, and three stations of silicon-strip

¹Throughout this paper, the notation D is used to refer to a D^+ , D^0 or D_s^+ meson, and B represents either a B^0 , B^- or B_s^0 meson.

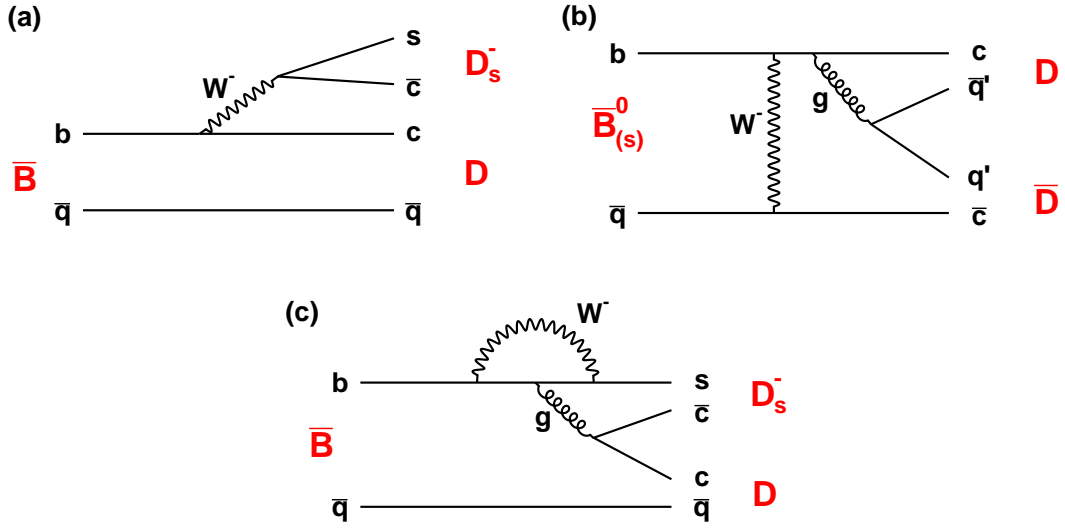


Figure 1: Feynman diagrams contributing to the double-charm final states discussed in this paper. They include (a) tree, (b) W -exchange and (c) penguin diagrams.

38 detectors and straw drift tubes placed downstream. The combined tracking system has a
 39 momentum resolution ($\Delta p/p$) that varies from 0.4% at 5 GeV/ c to 0.6% at 100 GeV/ c , and
 40 an impact parameter (IP) resolution of 20 μm for tracks with high transverse momentum
 41 (p_T). The impact parameter is defined as the distance of closest approach of a given
 42 particle to the primary pp interaction vertex (PV). Charged hadrons are identified using
 43 two ring-imaging Cherenkov detectors [23]. Photons, electrons and charged particles are
 44 identified by a calorimeter system consisting of scintillating-pad and preshower detectors,
 45 an electromagnetic calorimeter and a hadronic calorimeter. Muons are identified by a
 46 system composed of alternating layers of iron and multiwire proportional chambers.

47 The trigger [24] consists of a hardware stage, based on information from the calorimeter
 48 and muon systems, followed by a software stage that performs a partial event reconstruction
 49 (only tracks with $p_T > 0.5$ GeV/ c are reconstructed and used). The software trigger
 50 requires a two-, three- or four-track secondary vertex with a large track p_T sum and a
 51 significant displacement from any of the reconstructed PVs. At least one track must have
 52 $p_T > 1.7$ GeV/ c and IP χ^2 greater than 16 with respect to all PVs. The IP χ^2 is defined
 53 as the difference between the χ^2 of the PV reconstructed with and without the considered
 54 particle. A multivariate algorithm [25] is used to identify secondary vertices that originate
 55 from the decays of b hadrons.

56 For the ratios of branching fractions between modes with identical final states, no
 57 requirements are made on the hardware trigger decision. When the final states differ, a
 58 trigger selection is applied to facilitate the determination of the relative trigger efficiency.
 59 The selection requires that either (i) at least one of the tracks from the reconstructed
 60 signal decay is associated with energy depositions in the calorimeters that passed the
 61 hardware trigger requirements, or (ii) the event triggered independently of the signal decay

62 particles, *e.g.*, on the decay products of the other b hadron in the event. Events that do
 63 not fall into either of these two categories ($\sim 5\%$) are discarded.

64 Signal efficiencies and specific backgrounds are studied using simulated events. Proton-
 65 proton collisions are generated using PYTHIA 6.4 [26] with a specific LHCb configura-
 66 tion [27]. Decays of hadronic particles are described by EVTGEN [28] in which final state
 67 radiation is generated using PHOTOS [29]. The interaction of the generated particles
 68 with the detector and its response are implemented using the GEANT4 toolkit [30] as
 69 described in Ref. [31]. Efficiencies for identifying K^+ and π^+ mesons are determined using
 70 D^{*+} calibration data, with kinematic quantities reweighted to match those of the signal
 71 particles [23].

72 Signal B candidates are formed by combining pairs of D meson candidates recon-
 73 structed in the following decay modes: $D^0 \rightarrow K^-\pi^+$ or $K^-\pi^+\pi^-\pi^+$, $D^+ \rightarrow K^-\pi^+\pi^+$ and
 74 $D_s^+ \rightarrow K^+K^-\pi^+$. The $D^0 \rightarrow K^-\pi^+\pi^-\pi^+$ decay is only used for $\bar{B}_{(s)}^0 \rightarrow D^0\bar{D}^0$ candidates,
 75 where a single $D^0 \rightarrow K^-\pi^+\pi^-\pi^+$ decay in the final state is allowed, which approximately
 76 doubles the total signal efficiency. A refit of signal candidates with D mass and vertex
 77 constraints is performed to improve the B mass resolution.

78 Due to similar kinematics of the $D^+ \rightarrow K^-\pi^+\pi^+$, $D_s^+ \rightarrow K^+K^-\pi^+$ and $\Lambda_c^+ \rightarrow pK^-\pi^+$
 79 decays, there is cross-feed between various b -hadron decays that have two charm particles
 80 in the final state. Cross-feed between D^+ and D_s^+ occurs when the $K^-\pi^+h^+$ invariant
 81 mass is within 25 MeV/ c^2 (~ 3 times the experimental resolution) of both the D^+ and
 82 D_s^+ masses under the $h^+ = \pi^+$ and $h^+ = K^+$ hypotheses, respectively. In such cases,
 83 an arbitration is performed as follows: if either $|M(K^+K^-) - m_\phi| < 10$ MeV/ c^2 or h^+
 84 satisfies a stringent kaon particle identification (PID) requirement, the D candidate is
 85 assigned to be a D_s^+ meson. Conversely, if h^+ passes a stringent pion PID requirement,
 86 the D candidate is taken to be a D^+ meson. Candidates that do not pass either of these
 87 selections are rejected. A similar veto is applied to D^+ and D_s^+ decays that are consistent
 88 with the $\Lambda_c^+ \rightarrow pK^-\pi^+$ decay hypothesis if the proton is misidentified as a π^+ or K^+ ,
 89 respectively. The efficiencies of these D selections are determined using simulated signal
 90 decays to model the kinematics of the decay and $D^{*+} \rightarrow D^0\pi^+$ calibration data for the
 91 PID efficiencies. Their values are given in Table 1.

92 To suppress contributions from non- $D\bar{D}'$ final states, the reconstructed D decay vertex
 93 is required to be downstream of the reconstructed B decay vertex, and the B and D decay
 94 vertices are required to have a vertex separation (VS) χ^2 larger than two. Here, the VS χ^2
 95 is the difference in χ^2 between the nominal vertex fit and a vertex fit where the D is
 96 assumed to have zero lifetime. The efficiencies of this set of requirements are obtained
 97 from simulation and are included in Table 1.

98 To further improve the purity of the $B \rightarrow D\bar{D}'$ samples, a boosted decision tree
 99 (BDT) discriminant is used to distinguish signal D mesons from backgrounds [32,33]. The
 100 BDT uses five variables for the D meson and 23 for each of its children. The variables
 101 include kinematic quantities, track quality, and vertex and PID information. The signal
 102 and background distributions used to train the BDT are obtained from $\bar{B}^0 \rightarrow D^+\pi^-$,
 103 $B^- \rightarrow D^0\pi^-$ and $\bar{B}_s^0 \rightarrow D_s^+\pi^-$ decays from data. The signal distributions are background
 104 subtracted using weights [34] obtained from a fit to the B candidate invariant mass

Table 1: Individual contributions to the efficiency for selecting the various $B \rightarrow D\bar{D}'$ final states. Shown are the efficiencies to reconstruct and trigger on the final state, and to pass the charm cross-feed veto, the VS χ^2 and BDT selection requirements. The total selection efficiency is the product of these four values. The relative uncertainty on the selection efficiency for each decay mode due to the finite simulation samples sizes is 2%. Entries with a dash indicate that the efficiency factor is not applicable.

	Efficiencies (%)			
	Rec. \times Trig.	Cross-feed veto	VS χ^2	BDT
$\bar{B}_s^0 \rightarrow D_s^+ D_s^-$	0.140	88.4	75.4	97.5
$B^0 \rightarrow D_s^+ D^-$ (loose selection)	0.130	77.8	82.9	100.0
$\bar{B}_{(s)}^0 \rightarrow D^0 \bar{D}^0, (K^- \pi^+, K^+ \pi^-)$	0.447	–	73.7	57.8
$\bar{B}_{(s)}^0 \rightarrow D^0 \bar{D}^0, (K^- \pi^+, K^+ \pi^- \pi^+ \pi^-)$	0.128	–	74.6	63.6
$B^- \rightarrow D^0 D_s^-$	0.238	92.5	75.0	99.2

105 distribution. The background distributions are taken from the high B mass sidebands in
 106 the same data sample.

107 It is found that making a requirement on the product of the two D meson BDT responses
 108 provides better discrimination than applying one to each BDT response individually. The
 109 optimal BDT requirement in each decay is chosen by maximizing $N_S/\sqrt{N_S + N_B}$. The
 110 number of signal events, N_S , is computed using the known (or estimated, if unknown)
 111 branching fractions, selection efficiencies from simulated events, and the BDT efficiencies
 112 from the $\bar{B}^0 \rightarrow D^+ \pi^-$, $B^- \rightarrow D^0 \pi^-$ and $\bar{B}_s^0 \rightarrow D_s^+ \pi^-$ calibration samples, reweighted to
 113 account for small differences in kinematics between the calibration and signal samples.
 114 The number, N_B , is the expected background yield for a given BDT requirement. The
 115 efficiencies associated with the optimal BDT cut values, determined from an independent
 116 subset of the $B \rightarrow D\pi^-$ data, are listed in Table 1. Correlations between the BDT values
 117 for the two D mesons are taken into account.

118 For the purpose of measuring $\mathcal{B}(\bar{B}_s^0 \rightarrow D_s^+ D_s^-)/\mathcal{B}(B^0 \rightarrow D_s^+ D^-)$, only loose BDT
 119 requirements are imposed since the expected yields are relatively large. On the other hand,
 120 for $\mathcal{B}(\bar{B}_s^0 \rightarrow D_s^+ D^-)/\mathcal{B}(B^0 \rightarrow D_s^+ D^-)$, the expected signal yield of $\bar{B}_s^0 \rightarrow D_s^+ D^-$ decays is
 121 small; in this case both the signal and normalization modes are required to pass the same
 122 tighter BDT requirement. The different BDT selections applied to the $B^0 \rightarrow D_s^+ D^-$ decay
 123 are referred to as the “loose selection” and the “tight selection.” Since the final state
 124 is identical for the tight selection, the BDT efficiency cancels in the ratio of branching
 125 fractions, and is not included in Table 1.

126 For $\bar{B}_{(s)}^0 \rightarrow D^0 \bar{D}^0$ candidates, a peaking background from $B \rightarrow D^{*+} \pi^- \rightarrow (D^0 \pi^+) \pi^-$
 127 decays, where the π^+ is misidentified as a K^+ , is observed. This contribution is removed
 128 by requiring the mass difference, $M(K^- \pi^+ \pi^+) - M(K^- \pi^+) > 150$ MeV/ c^2 , where the K^+
 129 in the reconstructed decay is taken to be a π^+ . After the final selection around 2% of

130 events in the $\bar{B}_s^0 \rightarrow D_s^+ D_s^-$ decay mode contain multiple candidates; for all other modes
 131 the multiple candidate rate is below 1%. All candidates are kept for the final analysis.

132 3 Signal and background shapes

133 The $B \rightarrow D\bar{D}'$ signal shapes are all similar after the D mass and vertex constraints. The
 134 signal shape is parameterized as the sum of two Crystal Ball (CB) functions [35], which
 135 account for non-Gaussian tails on both sides of the signal peak. The asymmetric shapes
 136 account for both non-Gaussian mass resolution effects (on both sides) and energy loss
 137 due to final state radiation. The two CB shapes are constrained to have equal area and
 138 a common mean. Separate sets of shape parameters are determined for $B^0 \rightarrow D_s^+ D_s^-$,
 139 $\bar{B}_s^0 \rightarrow D_s^+ D_s^-$ and $B^- \rightarrow D^0 D_s^-$ using simulated signal decays. In the fits to data, the
 140 signal shape parameters are fixed to the simulated values, except for a smearing factor
 141 that is added in quadrature to the widths from simulation. This number is allowed to
 142 vary independently in each fit, but is consistent with about 4.6 MeV/ c^2 across all modes,
 143 resulting in a mass resolution of about 9 MeV/ c^2 . For the more rare $\bar{B}_{(s)}^0 \rightarrow D^0 \bar{D}^0$ and
 144 $\bar{B}_{(s)}^0 \rightarrow D^+ D^-$ decay modes, the $\bar{B}_s^0 \rightarrow D_s^+ D_s^-$ signal shape parameters are used. In
 145 determining the signal significances, the signal shape is fixed to that for $\bar{B}_s^0 \rightarrow D_s^+ D_s^-$,
 146 including an additional smearing of 4.6 MeV/ c^2 . The impact of using the $B^0 \rightarrow D_s^+ D^-$ or
 147 $B^- \rightarrow D^0 D_s^-$ signal shapes on the signal significances is negligible.

148 Several specific backgrounds contribute to the $D\bar{D}'$ mass spectra. In particular, decays
 149 such as $B \rightarrow D^{(*)} \bar{D}^*$, where the D^* mesons decay through pion or photon emission, produce
 150 distinct structures in all decays under consideration. The shapes of these backgrounds
 151 are derived from simulation, which are corrected for known resolution differences between
 152 data and simulated events, and then fixed in fits to the data. The relative yield of the two
 153 peaks in the characteristic structure from the decay $D^* \rightarrow D^0 \pi$ is allowed to vary freely, to
 154 enable better modeling of the background in the low mass region. Since this mass region
 155 is significantly below the signal peaks, the impact on the signal yield determinations is
 156 negligible.

157 A source of peaking background that contributes to $B \rightarrow DD_s^+$ modes are the
 158 $B \rightarrow D\bar{K}^{*0} K^+ \rightarrow DK^- \pi^+ K^+$ decays, where the $\bar{K}^{*0} K^+$ is not produced in a D_s^+ de-
 159 cay. Although the branching fractions for these decays [36] are about twice as large as
 160 that of the $B \rightarrow DD_s^+ \rightarrow DK^+ K^- \pi^+$ decay channel, the 25 MeV/ c^2 mass window around
 161 the known D_s^+ mass and the VS $\chi^2 > 2$ requirement reduce this contribution to about 1%
 162 of the signal yield. This expectation is corroborated by studying the D_s^+ candidate mass
 163 sidebands. The shape of this background is obtained from simulation, and is described
 164 by a single Gaussian function which has a width about 2.5 times larger than that of the
 165 signal decay and peaks at the nominal B meson mass.

166 After the charm cross-feed vetoes (see Sect. 2), the cross-feed rate from $B^0 \rightarrow D_s^+ D^-$
 167 decays into the $\bar{B}_s^0 \rightarrow D_s^+ D_s^-$ sample is $(0.7 \pm 0.2)\%$. The shape of this misidentification
 168 background is obtained from simulation. A similar cross-feed background contribution
 169 from $\Lambda_b^0 \rightarrow \Lambda_c^+ D_s^-$ decays is also expected due to events passing the Λ_c^+ veto. Taking

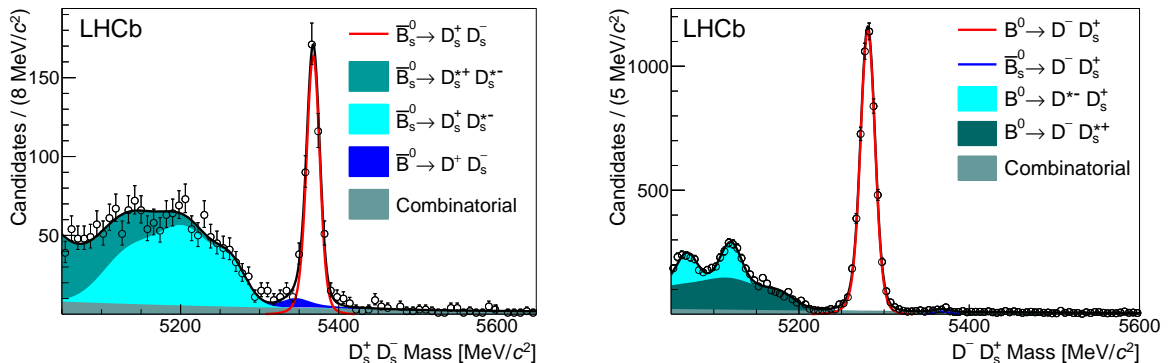


Figure 2: Invariant mass distributions for (left) $\bar{B}_s^0 \rightarrow D_s^+ D_s^-$ and (right) $B^0 \rightarrow D_s^+ D^-$ candidates in the data with the loose BDT selection applied to the latter. The signal and background components are indicated in the legend. The $\Lambda_b^0 \rightarrow \Lambda_c^+ D_s^-$, $\bar{B}_s^0 \rightarrow D_s^+ K^- K^+ \pi^-$ and $B^0 \rightarrow D^- K^+ K^- \pi^+$ background components are too small to be seen, and are excluded from the legends.

170 into account the observed yields of these decays in data, we fix the $B^0 \rightarrow D_s^+ D^-$ and
 171 $\Lambda_b^0 \rightarrow \Lambda_c^+ D_s^-$ cross-feed yields to 35 and 15 events, respectively. Investigation of the D
 172 mass sidebands reveals no additional contributions from non- DD' backgrounds.

173 The combinatorial background shape is described by an exponential function whose
 174 slope is determined from wrong-sign candidates. Wrong-sign candidates include the $D_s^+ D_s^+$,
 175 $D^0 D^0$, or $\bar{D}^0(K^+ \pi^-) D_s^-$ final states, in which no signal excesses should be present (ne-
 176 glecting the small contribution from the doubly Cabibbo suppressed $B^- \rightarrow D^0(K^+ \pi^-) D_s^-$
 177 decay). For the $\bar{B}_{(s)}^0 \rightarrow D^+ D^-$ decay, the exponential shape parameter is allowed to vary
 178 in the fit due to an insufficient number of wrong-sign $D^+ D^+$ candidates.

179 4 Fit results

180 Figure 2 shows the invariant mass spectra for $\bar{B}_s^0 \rightarrow D_s^+ D_s^-$ and $B^0 \rightarrow D_s^+ D^-$ candidates.
 181 The results of unbinned extended maximum likelihood fits to the distributions are overlaid
 182 with the signal and background components indicated in the legends. Signal yields of
 183 451 ± 23 $\bar{B}_s^0 \rightarrow D_s^+ D_s^-$ and 5157 ± 64 $B^0 \rightarrow D_s^+ D^-$ decays are observed.

184 Figure 3 shows the invariant mass spectrum for $B^0 \rightarrow D_s^+ D^-$ and $\bar{B}_s^0 \rightarrow D_s^+ D^-$
 185 candidates, where the tight BDT selection requirements have been applied as discussed
 186 previously. We observe 36 ± 6 $\bar{B}_s^0 \rightarrow D_s^+ D^-$ signal decays, with 2832 ± 53 events in
 187 the $B^0 \rightarrow D_s^+ D^-$ normalization mode. The statistical significance of the $\bar{B}_s^0 \rightarrow D_s^+ D^-$
 188 signal corresponds to 10σ by computing $\sqrt{-2 \ln(\mathcal{L}_0/\mathcal{L}_{\max})}$, where \mathcal{L}_{\max} and \mathcal{L}_0 are the fit
 189 likelihoods with the signal yields allowed to vary and fixed to zero, respectively. Variations
 190 in the signal and background model have only a marginal impact on the signal significance.
 191 The $\bar{B}_s^0 \rightarrow D^- D_s^+$ decay is thus observed for the first time.

192 The invariant mass spectrum for $\bar{B}_{(s)}^0 \rightarrow D^+ D^-$ candidates is shown in Fig. 4 (left).

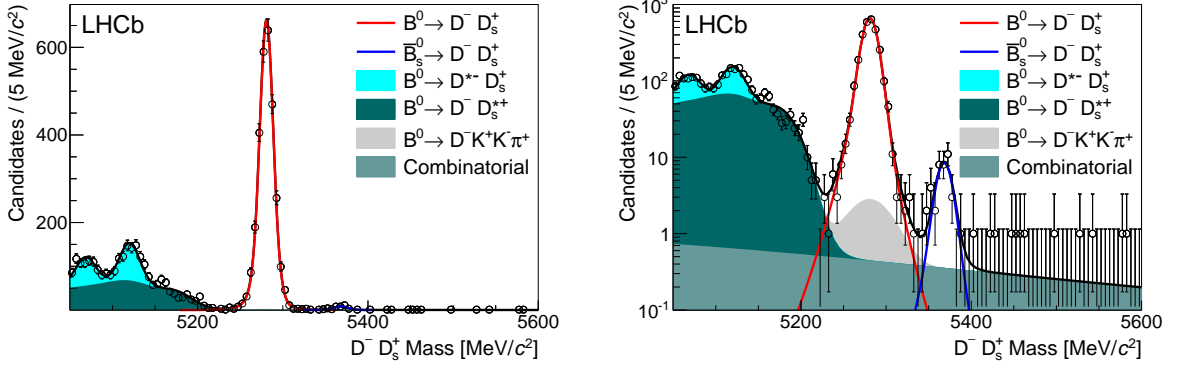


Figure 3: Invariant mass distribution for $B^0 \rightarrow D_s^+ D^-$ and $\bar{B}_s^0 \rightarrow D_s^+ D^-$ candidates in the data, with the tight BDT selection applied. The distribution is plotted on a (left) linear and (right) logarithmic scale to highlight the suppressed $\bar{B}_s^0 \rightarrow D_s^+ D^-$ signal. Signal and background components are indicated in the legend.

193 Peaks are seen at both the B^0 and B_s^0 meson masses, with yields of 165 ± 13 and 43 ± 7 signal
 194 events, respectively. In the lower mass region, two prominent peaks from $\bar{B}^0 \rightarrow D^{*+} D^-$ and
 195 $\bar{B}^0 \rightarrow D^+ D^{*-}$ decays are also evident. The significance of the $\bar{B}_s^0 \rightarrow D^+ D^-$ signal yield is
 196 computed as described above, and corresponds to 11σ , establishing the first observation of
 197 this decay mode.

198 Figure 4 (right) shows the $D^0 \bar{D}^0$ invariant mass distribution and the results of the fit.
 199 Both $(K^- \pi^+, K^+ \pi^-)$ and $(K^- \pi^+, K^+ \pi^- \pi^+ \pi^-)$ combinations are included. A $\bar{B}_s^0 \rightarrow D^0 \bar{D}^0$
 200 signal is seen with a significance of 11σ , which establishes the first observation of this
 201 decay mode. The data also show an excess of events at the B^0 mass. The significance of
 202 that excess corresponds to 2.4σ , including both the statistical and systematic uncertainty.
 203 The fitted yields in the $\bar{B}_s^0 \rightarrow D^0 \bar{D}^0$ and $\bar{B}^0 \rightarrow D^0 \bar{D}^0$ decay modes are 45 ± 8 and
 204 13 ± 6 events, respectively. If both the $\bar{B}_s^0 \rightarrow D^0 \bar{D}^0$ and $\bar{B}^0 \rightarrow D^0 \bar{D}^0$ decays proceed
 205 through W -exchange diagrams, one would expect the signal yield in $\bar{B}^0 \rightarrow D^0 \bar{D}^0$ to be
 206 $\sim (f_d/f_s) \times |V_{cd}/V_{cs}|^2 \simeq 0.2$ of the yield in $\bar{B}_s^0 \rightarrow D^0 \bar{D}^0$, where we have used $|V_{cd}/V_{cs}|^2 =$
 207 0.054 [18] and $f_s/f_d = 0.256 \pm 0.020$ [37]. The fitted yields are consistent with this
 208 expectation. The decay $B^- \rightarrow D^0 D_s^-$ is used as the normalization channel for both
 209 the $\bar{B}_s^0 \rightarrow D^0 \bar{D}^0$ and $\bar{B}^0 \rightarrow D^0 \bar{D}^0$ branching fraction measurements, where only the
 210 $D^0 \rightarrow K^- \pi^+$ decay mode is used. The fitted invariant mass distribution for $B^- \rightarrow D^0 D_s^-$
 211 candidates is shown in Fig. 5. The fitted signal yield is 5152 ± 73 events.

212 The measured yields, $N_{B \rightarrow D \bar{D}'}$, relevant for the branching fraction measurements are

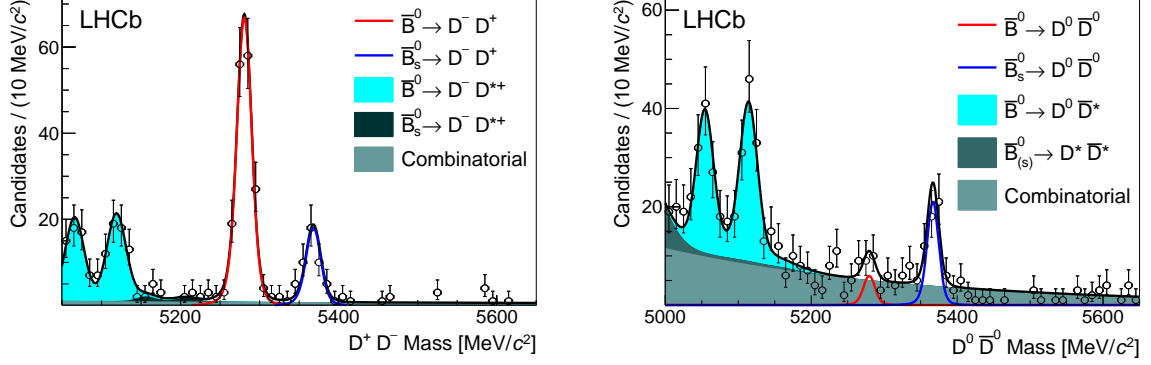


Figure 4: Invariant mass distributions for (left) $\bar{B}_{(s)}^0 \rightarrow D^+ D^-$ and (right) $\bar{B}_{(s)}^0 \rightarrow D^0 \bar{D}^0$ candidates in the data. Signal and background components are indicated in the legend.

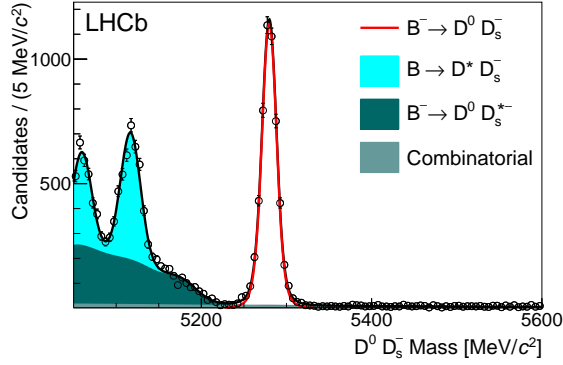


Figure 5: Invariant mass distribution for $B^- \rightarrow D^0 \bar{D}_s^-$ candidates in the data. Signal and background components are indicated in the legend. The $B^- \rightarrow D^0 K^- K^+ \pi^-$ background components are too small to be seen, and are excluded from the legend.

213 summarized in Table 2. The branching fractions are related to the measured yields by

$$\frac{\mathcal{B}(\bar{B}_s^0 \rightarrow D_s^+ D_s^-)}{\mathcal{B}(B^0 \rightarrow D_s^+ D^-)} = \frac{f_d}{f_s} \cdot \epsilon_{\text{rel}}^{B^0/B_s^0} \cdot \kappa \cdot \frac{\mathcal{B}(D^+ \rightarrow K^- \pi^+ \pi^+)}{\mathcal{B}(D_s^+ \rightarrow K^+ K^- \pi^+)}, \quad (1)$$

$$\frac{\mathcal{B}(\bar{B}_s^0 \rightarrow D_s^+ D^-)}{\mathcal{B}(B^0 \rightarrow D_s^+ D^-)} = \frac{f_d}{f_s} \cdot \epsilon_{\text{rel}} \cdot \frac{N_{\bar{B}_s^0 \rightarrow D_s^+ D^-}}{N_{B^0 \rightarrow D_s^+ D^-}}, \quad (2)$$

$$\frac{\mathcal{B}(\bar{B}_s^0 \rightarrow D^+ D^-)}{\mathcal{B}(\bar{B}^0 \rightarrow D^+ D^-)} = \frac{f_d}{f_s} \cdot \epsilon_{\text{rel}} \cdot \kappa \cdot \frac{N_{\bar{B}_s^0 \rightarrow D^+ D^-}}{N_{\bar{B}^0 \rightarrow D^+ D^-}}, \quad (3)$$

$$\frac{\mathcal{B}(\bar{B}_s^0 \rightarrow D^0 \bar{D}^0)}{\mathcal{B}(B^- \rightarrow D^0 \bar{D}_s^-)} = \frac{f_d}{f_s} \cdot \epsilon'_{\text{rel}} \cdot \kappa \cdot \frac{N_{\bar{B}_s^0 \rightarrow D^0 \bar{D}^0}}{N_{B^- \rightarrow D^0 \bar{D}_s^-}}, \quad (4)$$

$$\frac{\mathcal{B}(\bar{B}^0 \rightarrow D^0 \bar{D}^0)}{\mathcal{B}(B^- \rightarrow D^0 \bar{D}_s^-)} = \epsilon'_{\text{rel}} \cdot \frac{N_{\bar{B}^0 \rightarrow D^0 \bar{D}^0}}{N_{B^- \rightarrow D^0 \bar{D}_s^-}}, \quad (5)$$

Table 2: Summary of the observed signal and normalization mode yields and their relative efficiencies, as used in the measurements of the ratios of branching fractions. The quoted uncertainties are statistical only.

Measurement	Signal yield	Norm. yield	Rel. eff. $\epsilon_{\text{rel}}^{(\prime)}$
$\frac{\mathcal{B}(\bar{B}_s^0 \rightarrow D_s^+ D_s^-)}{\mathcal{B}(B^0 \rightarrow D_s^+ D^-)}$	451 ± 23	5157 ± 64	0.928 ± 0.027
$\frac{\mathcal{B}(\bar{B}_s^0 \rightarrow D_s^+ D^-)}{\mathcal{B}(B^0 \rightarrow D_s^+ D^-)}$	36 ± 6	2832 ± 53	1.0
$\frac{\mathcal{B}(\bar{B}_s^0 \rightarrow D^+ D^-)}{\mathcal{B}(\bar{B}^0 \rightarrow D^+ D^-)}$	43 ± 7	165 ± 13	1.0
$\frac{\mathcal{B}(\bar{B}_s^0 \rightarrow D^0 \bar{D}^0)}{\mathcal{B}(B^- \rightarrow D^0 D_s^-)}$	45 ± 8	5152 ± 73	0.523 ± 0.016
$\frac{\mathcal{B}(\bar{B}^0 \rightarrow D^0 \bar{D}^0)}{\mathcal{B}(B^- \rightarrow D^0 D_s^-)}$	13 ± 6	5152 ± 73	0.523 ± 0.016
$\frac{\mathcal{B}(B^- \rightarrow D^0 D_s^-)}{\mathcal{B}(B^0 \rightarrow D_s^+ D^-)}$	5152 ± 73	5157 ± 64	0.508 ± 0.011

$$\frac{\mathcal{B}(B^- \rightarrow D^0 D_s^-)}{\mathcal{B}(B^0 \rightarrow D_s^+ D^-)} = \epsilon_{\text{rel}}^{B^0/B^-} \cdot \frac{\mathcal{B}(D^+ \rightarrow K^- \pi^+ \pi^+)}{\mathcal{B}(D^0 \rightarrow K^- \pi^+)} \cdot \frac{N_{B^- \rightarrow D^0 D_s^-}}{N_{B^0 \rightarrow D_s^+ D^-}}. \quad (6)$$

214 Here, it is assumed that B^- and \bar{B}^0 mesons are produced in equal numbers. The relative
 215 efficiencies, ϵ_{rel} , are given in Table 2. They account for geometric acceptance, detection and
 216 trigger efficiencies, and the additional VS χ^2 , BDT, and charm cross-feed veto requirements.
 217 The first four of these relative efficiencies are obtained from simulation, and the last two
 218 are data-driven. The indicated uncertainties on the relative efficiencies are due only to the
 219 finite sizes of the simulated signal decays. The average selection efficiency for $B^- \rightarrow D^0 D_s^-$
 220 relative to $\bar{B}_{(s)}^0 \rightarrow D^0 \bar{D}^0$ is

$$\epsilon'_{\text{rel}} = \frac{\epsilon_{B^- \rightarrow D^0 D_s^-} \mathcal{B}(D_s^+ \rightarrow K^+ K^- \pi^+) \mathcal{B}(D^0 \rightarrow K^- \pi^+)}{\epsilon_{K\pi, K\pi} [\mathcal{B}(D^0 \rightarrow K^- \pi^+)]^2 + 2\epsilon_{K\pi\pi\pi, K\pi} \mathcal{B}(D^0 \rightarrow K^- \pi^+) \mathcal{B}(D^0 \rightarrow K^- \pi^+ \pi^- \pi^+)}, \quad (7)$$

221 where the quantities $\epsilon_{B^- \rightarrow D^0 D_s^-} = (0.166 \pm 0.003)\%$, $\epsilon_{K\pi, K\pi} = (0.190 \pm 0.003)\%$
 222 and $\epsilon_{K\pi\pi\pi, K\pi} = (0.061 \pm 0.002)\%$ are the selection efficiencies for the $B^- \rightarrow D^0 D_s^-$,
 223 $\bar{B}_s^0 \rightarrow (D^0 \rightarrow K^- \pi^+, \bar{D}^0 \rightarrow K^+ \pi^-)$ and $\bar{B}_s^0 \rightarrow (D^0 \rightarrow K^- \pi^+, \bar{D}^0 \rightarrow K^+ \pi^- \pi^+ \pi^-)$ de-
 224 cays, respectively. The D branching fractions, $\mathcal{B}(D^0 \rightarrow K^- \pi^+) = (3.88 \pm 0.05)\%$,
 225 $\mathcal{B}(D^0 \rightarrow K^- \pi^+ \pi^- \pi^+) = (8.07 \pm 0.20)\%$, $\mathcal{B}(D_s^+ \rightarrow K^+ K^- \pi^+) = (5.49 \pm 0.27)\%$, and
 226 $\mathcal{B}(D^+ \rightarrow K^- \pi^+ \pi^+) = (9.13 \pm 0.19)\%$ are taken from Ref. [18].

227 The factor κ is a correction that accounts for the lower selection efficiency associated
 228 with the shorter-lifetime CP -even eigenstates of the B_s^0 system compared to flavor-specific
 229 final states [14]. The impact on the B_s^0 acceptance is estimated by convolving an exponential
 230 distribution that has a 10% smaller lifetime than that in flavor-specific decays with the

231 simulated lifetime acceptance. The resulting correction is $\kappa = 1.058 \pm 0.029$. In the B^0
 232 sector, $\Delta\Gamma_d/\Gamma_d$ is below 1% [38], and the lifetime acceptance is well described by the
 233 simulation.

234 The measured ratios of branching fractions are computed to be

$$\begin{aligned} \frac{\mathcal{B}(\bar{B}_s^0 \rightarrow D^+ D^-)}{\mathcal{B}(\bar{B}^0 \rightarrow D^+ D^-)} &= 1.08 \pm 0.20 \text{ (stat)} \pm 0.10 \text{ (syst)}, \\ \frac{\mathcal{B}(\bar{B}_s^0 \rightarrow D_s^+ D^-)}{\mathcal{B}(B^0 \rightarrow D_s^+ D^-)} &= 0.050 \pm 0.008 \text{ (stat)} \pm 0.004 \text{ (syst)}, \\ \frac{\mathcal{B}(\bar{B}_s^0 \rightarrow D^0 \bar{D}^0)}{\mathcal{B}(B^- \rightarrow D^0 D_s^-)} &= 0.019 \pm 0.003 \text{ (stat)} \pm 0.003 \text{ (syst)}, \\ \frac{\mathcal{B}(\bar{B}^0 \rightarrow D^0 \bar{D}^0)}{\mathcal{B}(B^- \rightarrow D^0 D_s^-)} &= 0.0014 \pm 0.0006 \text{ (stat)} \pm 0.0002 \text{ (syst)} \\ &[< 0.0024 \text{ at } 90\% \text{ CL }], \\ \frac{\mathcal{B}(\bar{B}_s^0 \rightarrow D_s^+ D_s^-)}{\mathcal{B}(B^0 \rightarrow D_s^+ D^-)} &= 0.56 \pm 0.03 \text{ (stat)} \pm 0.04 \text{ (syst)}, \\ \frac{\mathcal{B}(B^- \rightarrow D^0 D_s^-)}{\mathcal{B}(B^0 \rightarrow D_s^+ D^-)} &= 1.22 \pm 0.02 \text{ (stat)} \pm 0.07 \text{ (syst)}. \end{aligned}$$

235 For $\mathcal{B}(\bar{B}_s^0 \rightarrow D^0 \bar{D}^0)/\mathcal{B}(B^- \rightarrow D^0 D_s^-)$, the results obtained using the
 236 $D^0(K^-\pi^+)\bar{D}^0(K^+\pi^-\pi^+\pi^-)$ and $D^0(K^-\pi^+)\bar{D}^0(K^+\pi^-)$ final states differ by less
 237 than one standard deviation. For the $\bar{B}^0 \rightarrow D^0 \bar{D}^0$ decay, we provide both the central value
 238 and the 90% confidence level (CL) upper limit. The upper limit is obtained by convolving
 239 the fitted likelihood with a Gaussian function whose width is the total systematic error,
 240 and integrating over the physical region.

241 5 Systematic uncertainties

242 A number of systematic uncertainties contribute to the measurements of the ratios of
 243 branching fractions. The sources and their values are summarized in Table 3. The dominant
 244 source of uncertainty on the branching fraction ratios comes from the b fragmentation
 245 fraction ratio, f_d/f_s , which has a total uncertainty of 7.8% [37], of which 5.3% is from the
 246 ratio of branching fractions $\mathcal{B}(D_s^+ \rightarrow K^+ K^- \pi^+)/\mathcal{B}(D^+ \rightarrow K^- \pi^+ \pi^+)$. For clarity, we have
 247 removed that portion of the uncertainty from f_d/f_s , and included its contribution in the
 248 row labeled $\mathcal{B}(D)$ in Table 3. For $\mathcal{B}(\bar{B}_s^0 \rightarrow D_s^+ D_s^-)/\mathcal{B}(B^0 \rightarrow D_s^+ D^-)$, the above D_s^+/D^+
 249 branching fraction ratio from f_d/f_s cancels with the corresponding inverted ratio in Eq. 1.
 250 On the other hand, in the ratio $\mathcal{B}(\bar{B}_{(s)}^0 \rightarrow D^0 \bar{D}^0)/\mathcal{B}(B^- \rightarrow D^0 D_s^-)$, the $D_s^+ \rightarrow K^+ K^- \pi^+$
 251 branching fraction enters as the square, after considering the D branching fractions used
 252 in computing f_d/f_s (see Eq. 4). As a result, the uncertainty from $\mathcal{B}(D_s^+ \rightarrow K^+ K^- \pi^+)$
 253 contributes 9.8% to the total uncertainty on $\mathcal{B}(\bar{B}_{(s)}^0 \rightarrow D^0 \bar{D}^0)/\mathcal{B}(B^- \rightarrow D^0 D_s^-)$; smaller

254 contributions from the limited knowledge of $\mathcal{B}(D^0 \rightarrow K^- \pi^+)$ [1.3%], $\mathcal{B}(D^0 \rightarrow K^- \pi^+ \pi^- \pi^+)$
 255 [2.5%] and $\mathcal{B}(D^+ \rightarrow K^- \pi^+ \pi^+)$ [2.1%] are also included in the $\mathcal{B}(D)$ uncertainties.

256 Another significant uncertainty results from the precision on b -hadron lifetimes and
 257 decays of B^0 and B_s^0 to CP eigenstates. Using the measured value of the width difference,
 258 $\Delta\Gamma_s = 0.116 \pm 0.018 \pm 0.006 \text{ ps}^{-1}$ [39] we conservatively assume the CP -even lifetime to
 259 be in the range from 0.85 to 0.95 times the flavor-specific decay lifetime. With this allowed
 260 range a 2.9% uncertainty on the efficiencies for \bar{B}_s^0 decays to CP eigenstates is found. The
 261 average B_s^0 lifetime is known only to a precision of 3%, which leads to a 1.5% uncertainty
 262 on the selection efficiencies for B_s^0 decays to flavor-specific final states. The B^0 and B^-
 263 lifetimes are known with sufficient precision that the associated uncertainty is negligible.

264 Several of the efficiency factors are estimated from simulation. Most, but not all, of
 265 the associated systematic uncertainties cancel due to the similar or identical final states
 266 for the signal and normalization modes. For modes with an unequal number of tracks
 267 in the final state, a 1% uncertainty due to small differences in the IP resolution between
 268 data and simulation is assigned. The efficiency of the VS χ^2 requirement is checked
 269 using the large $B^0 \rightarrow D_s^+ D^-$ signal in data, and the agreement to within 1% with the
 270 efficiency from simulation is the assigned uncertainty. For $\mathcal{B}(B^- \rightarrow D^0 D_s^-)/\mathcal{B}(B^0 \rightarrow$
 271 $D_s^+ D^-)$, a 1% uncertainty is attributed to the efficiency of track reconstruction. For
 272 $\mathcal{B}(\bar{B}_s^0 \rightarrow D^0 \bar{D}^0)/\mathcal{B}(B^- \rightarrow D^0 D_s^-)$, the one fewer track in the $D^0(K\pi)\bar{D}^0(K\pi)$ final state is
 273 offset by the one extra track in $D^0(K\pi)\bar{D}^0(K\pi\pi\pi)$, relative to $D^0(K\pi)D_s^-(KK\pi)$, leading
 274 to a negligible tracking uncertainty. The mass resolution in data is slightly larger than
 275 in simulation, resulting in slightly different efficiencies for the reconstructed D^0 , D^+ and
 276 D_s^+ invariant masses to lie within 25 MeV/ c^2 of their known masses. This introduces
 277 a maximum of 1% uncertainty on the relative branching fractions. To estimate the
 278 uncertainty on the trigger efficiencies determined from simulation, the hadron trigger
 279 efficiency ratios were also determined using data. These efficiencies were measured using
 280 trigger-unbiased samples of kaons and pions identified in $D^{*+} \rightarrow D^0 \pi^+$ decays. Using
 281 this alternative procedure, we find that the simulated trigger efficiency ratios have an
 282 uncertainty of 2%. The combined systematic uncertainties in the efficiencies obtained from
 283 simulation are given in Table 3.

284 The limited sizes of the $B \rightarrow D\pi^-$ calibration samples lead to uncertainties in the
 285 BDT efficiencies. The uncertainties on the ratios vary from 1.0% to 2.0%. The uncertainty
 286 on the efficiency of the $D_{(s)}$ and Λ_c^+ vetoes is dominated by the PID efficiencies, but they
 287 only apply to the subset of D candidates that fall within the mass window of two charm
 288 hadrons, *e.g.*, both the D^+ and D_s^+ mesons, which occurs about 20% of the time for D_s^+
 289 decays. Taking this fraction and the uncertainty in the PID efficiency into account, the
 290 veto efficiencies are estimated to have uncertainties of 1.0% for the D^+ veto, 0.5% for the
 291 D_s^+ veto, and 0.3% for the Λ_c^+ veto.

292 The fit model is validated using simulated experiments, and is found to be unbiased.
 293 To assess the uncertainty due to the imperfect knowledge of the various parameters
 294 used in the fit model, a number of variations are investigated. The only non-negligible
 295 uncertainties are due to the $B \rightarrow DK^- K^+ \pi^-$ background contribution, which is varied
 296 from 0% to 2%, and the cross-feed from $\bar{B}_s^0 \rightarrow D_s^+ D^-$ decays into the $\bar{B}_s^0 \rightarrow D_s^+ D_s^-$ sample.

Table 3: Sources of systematic uncertainty and their values (in %) for the ratios of branching fractions of the indicated decays. For $\mathcal{B}(\bar{B}_{(s)}^0 \rightarrow D^0 \bar{D}^0)/\mathcal{B}(B^- \rightarrow D^0 D_s^-)$, the error on f_d/f_s only applies to the $\bar{B}_s^0 \rightarrow D^0 \bar{D}^0$ decay, as indicated by the values in parentheses.

Source	$\frac{\bar{B}_s^0 \rightarrow D_s^+ D_s^-}{B^0 \rightarrow D_s^+ D^-}$	$\frac{\bar{B}_s^0 \rightarrow D_s^+ D^-}{B^0 \rightarrow D_s^+ D^-}$	$\frac{\bar{B}_s^0 \rightarrow D^+ D^-}{\bar{B}^0 \rightarrow D^+ D^-}$	$\frac{\bar{B}_{(s)}^0 \rightarrow D^0 \bar{D}^0}{B^- \rightarrow D^0 D_s^-}$	$\frac{B^- \rightarrow D^0 D_s^-}{B^0 \rightarrow D_s^+ D^-}$
f_d/f_s	5.7	5.7	5.7	– (5.7)	–
$\mathcal{B}(D)$	–	5.3	5.3	10.2	2.5
B meson lifetimes	2.9	1.5	2.9	2.9	–
Eff. from simulation	2.4	–	–	2.2	2.6
BDT selection	1.4	–	–	2.2	1.4
Cross-feed vetoes	0.6	–	–	0.5	1.0
D mass resolution	1.0	–	–	1.0	1.0
Fit model	2.1	0.5	0.5	1.7	2.1
Simulated sample size	3.0	3.0	3.0	3.0	3.0
Total	8.0	8.5	8.9	11.7 (13.0)	5.5

297 The uncertainty varies from 1.7% to 2.1%. For $\mathcal{B}(\bar{B}_s^0 \rightarrow D^+ D^-)/\mathcal{B}(\bar{B}^0 \rightarrow D^+ D^-)$ and
 298 $\mathcal{B}(\bar{B}_s^0 \rightarrow D_s^+ D^-)/\mathcal{B}(B^0 \rightarrow D_s^+ D^-)$, we assign an uncertainty of 0.5%, which accounts for
 299 potentially small differences in the signal shape for \bar{B}^0 and \bar{B}_s^0 decays (due to the B^0 - B_s^0
 300 mass difference). Lastly, the finite size of the samples of simulated decays contributes
 301 3% uncertainty to all the measurements. In total, the systematic uncertainties on the
 302 branching fraction ratios range from 5.5% to 13.0%, as indicated in Table 3.

303 6 Discussion and summary

304 First observations and measurements of the relative branching fractions for the decays
 305 $\bar{B}_s^0 \rightarrow D^+ D^-$, $\bar{B}_s^0 \rightarrow D_s^+ D^-$ and $\bar{B}_s^0 \rightarrow D^0 \bar{D}^0$ have been presented, along with measure-
 306 ments of $\mathcal{B}(\bar{B}_s^0 \rightarrow D_s^+ D_s^-)$ and $\mathcal{B}(B^- \rightarrow D^0 D_s^-)$. Taking the world average values for
 307 $\mathcal{B}(B^0 \rightarrow D_s^+ D^-) = (7.2 \pm 0.8) \times 10^{-3}$ [18], the absolute branching fractions are

$$\begin{aligned} \mathcal{B}(B^- \rightarrow D^0 D_s^-) &= (8.6 \pm 0.2 \text{ (stat)} \pm 0.4 \text{ (syst)} \pm 1.0 \text{ (norm)}) \times 10^{-3}, \\ \mathcal{B}(\bar{B}_s^0 \rightarrow D_s^+ D_s^-) &= (4.0 \pm 0.2 \text{ (stat)} \pm 0.3 \text{ (syst)} \pm 0.4 \text{ (norm)}) \times 10^{-3}. \end{aligned}$$

308 The third uncertainty reflects the precision of the branching fraction for the normaliza-
 309 tion mode. These measurements are consistent with, and more precise than, both the
 310 current world average measurements [18] as well as the more recent measurement of
 311 $\mathcal{B}(\bar{B}_s^0 \rightarrow D_s^+ D_s^-)$ [40].

312 The measured value of $\mathcal{B}(\bar{B}_s^0 \rightarrow D_s^+ D_s^-)/\mathcal{B}(B^0 \rightarrow D_s^+ D^-) = 0.55 \pm 0.06$ is signif-
 313 icantly lower than the naive expectation of unity for the case that both decays are
 314 dominated by tree amplitudes (see Fig. 1(a)), assuming small non-factorizable effects and

315 comparable magnitudes of the $B_{(s)} \rightarrow D_{(s)}^+$ form factors [41]. Unlike $B^0 \rightarrow D_s^+ D^-$, the
 316 $\bar{B}_s^0 \rightarrow D_s^+ D_s^-$ decay receives a contribution from the W -exchange process (see Fig. 1(b)),
 317 suggesting that this amplitude may not be negligible. Interestingly, when comparing the
 318 $\bar{B}_s^0 \rightarrow D_s^+ D_s^-$ and $\bar{B}^0 \rightarrow D^+ D^-$ decays, which have the same set of amplitudes, one finds
 319 $|V_{cd}/V_{cs}|^2 \cdot \mathcal{B}(\bar{B}_s^0 \rightarrow D_s^+ D_s^-)/\mathcal{B}(\bar{B}^0 \rightarrow D^+ D^-) \sim 1$.

320 Using $\mathcal{B}(\bar{B}^0 \rightarrow D^+ D^-) = (2.11 \pm 0.31) \times 10^{-4}$ and $\mathcal{B}(B^- \rightarrow D^0 D_s^-) = (10.0 \pm 1.7) \times$
 321 10^{-3} [18], the following values for the branching fractions are obtained

$$\begin{aligned} \mathcal{B}(\bar{B}_s^0 \rightarrow D^+ D^-) &= (2.2 \pm 0.4 \text{ (stat)} \pm 0.2 \text{ (syst)} \pm 0.3 \text{ (norm)}) \times 10^{-4}, \\ \mathcal{B}(\bar{B}_s^0 \rightarrow D^0 \bar{D}^0) &= (1.9 \pm 0.3 \text{ (stat)} \pm 0.3 \text{ (syst)} \pm 0.3 \text{ (norm)}) \times 10^{-4}, \\ \mathcal{B}(\bar{B}^0 \rightarrow D^0 \bar{D}^0) &= (1.4 \pm 0.6 \text{ (stat)} \pm 0.2 \text{ (syst)} \pm 0.2 \text{ (norm)}) \times 10^{-5}. \end{aligned}$$

322 The first of these results disfavors the predicted values for $\mathcal{B}(\bar{B}_s^0 \rightarrow D^+ D^-)$ in Refs. [20,21],
 323 which are about 5–15 times larger than our measured value. The measured branching
 324 fractions are about a factor of 2–3 larger than the predictions obtained by assuming that
 325 these decay amplitudes are dominated by rescattering [17]. As discussed above for the
 326 $\mathcal{B}(\bar{B}_s^0 \rightarrow D_s^+ D_s^-)$ measurement, this may also suggest that the W -exchange amplitude
 327 contribution is not negligible in $B \rightarrow D\bar{D}'$ decays. For precise quantitative comparisons of
 328 these B_s^0 branching fraction measurements to theoretical predictions, one should account
 329 for the different total widths of the CP -even and CP -odd final states [12].

330 The Cabibbo suppressed $\bar{B}_s^0 \rightarrow D_s^+ D^-$ decay is also observed for the first time. Its
 331 absolute branching fraction is

$$\mathcal{B}(\bar{B}_s^0 \rightarrow D_s^+ D^-) = (3.6 \pm 0.6 \text{ (stat)} \pm 0.3 \text{ (syst)} \pm 0.4 \text{ (norm)}) \times 10^{-4}.$$

332 This value is consistent with the expected suppression of $|V_{cd}/V_{cs}|^2$.

333 The results reported here are based on an integrated luminosity of 1.0 fb^{-1} . A data
 334 sample with approximately 2.5 times larger yields in these modes has already been collected
 335 in 2012, and larger samples are anticipated in the next few years. These samples give
 336 good prospects for CP -violation measurements, lifetime studies, and obtaining a deeper
 337 understanding of the decay mechanisms that contribute to b -hadron decays.

338 Acknowledgements

339 We express our gratitude to our colleagues in the CERN accelerator departments for
 340 the excellent performance of the LHC. We thank the technical and administrative staff
 341 at the LHCb institutes. We acknowledge support from CERN and from the national
 342 agencies: CAPES, CNPq, FAPERJ and FINEP (Brazil); NSFC (China); CNRS/IN2P3
 343 and Region Auvergne (France); BMBF, DFG, HGF and MPG (Germany); SFI (Ireland);
 344 INFN (Italy); FOM and NWO (The Netherlands); SCSR (Poland); ANCS/IFA (Romania);
 345 MinES, Rosatom, RFBR and NRC “Kurchatov Institute” (Russia); MinECo, XuntaGal
 346 and GENCAT (Spain); SNSF and SER (Switzerland); NAS Ukraine (Ukraine); STFC
 347 (United Kingdom); NSF (USA). We also acknowledge the support received from the ERC

348 under FP7. The Tier1 computing centres are supported by IN2P3 (France), KIT and
 349 BMBF (Germany), INFN (Italy), NWO and SURF (The Netherlands), PIC (Spain),
 350 GridPP (United Kingdom). We are thankful for the computing resources put at our
 351 disposal by Yandex LLC (Russia), as well as to the communities behind the multiple open
 352 source software packages that we depend on.

353 References

- 354 [1] N. Cabibbo, *Unitary symmetry and leptonic decays*, Phys. Rev. Lett. **10** (1963) 531.
- 355 [2] M. Kobayashi and T. Maskawa, *CP violation in the renormalizable theory of weak*
 356 *interaction*, Prog. Theor. Phys. **49** (1973) 652.
- 357 [3] BaBar collaboration, B. Aubert *et al.*, *Measurements of time-dependent CP asymme-*
 358 *tries in $B^0 \rightarrow D^{(*)+}D^{(*)-}$ decays*, Phys. Rev. **D79** (2009) 032002, arXiv:0808.1866.
- 359 [4] Belle collaboration, S. Fratina *et al.*, *Evidence for CP violation in $B^0 \rightarrow D^+D^-$*
 360 *decays*, Phys. Rev. Lett. **98** (2007) 221802, arXiv:hep-ex/0702031.
- 361 [5] R. Aleksan *et al.*, *The decay $B \rightarrow D\bar{D}^* + D^*\bar{D}$ in the heavy quark limit and tests of*
 362 *CP violation*, Phys. Lett. **B317** (1993) 173.
- 363 [6] A. I. Sanda and Z. Z. Xing, *Towards determining ϕ_1 with $B \rightarrow D^{(*)}\bar{D}^{(*)}$* , Phys. Rev.
 364 **D56** (1997) 341, arXiv:hep-ph/9702297.
- 365 [7] Z. Z. Xing, *Measuring CP violation and testing factorization in $B_d \rightarrow D^{*\pm}D^{*\mp}$ and*
 366 *$B_s \rightarrow D_s^{*\pm}D_s^{*\mp}$ decays*, Phys. Lett. **B443** (1998) 365, arXiv:hep-ph/9809496.
- 367 [8] Z. Z. Xing, *CP violation in $B_d \rightarrow D^+D^-$, $D^{*+}D^-$, D^+D^{*-} , and $D^{*+}D^{*-}$ decays*,
 368 Phys. Rev. **D61** (2000) 014010, arXiv:hep-ph/9907455.
- 369 [9] X. Y. Pham and Z. Z. Xing, *CP asymmetries in $B_d \rightarrow D^{*+}D^{*-}$ and $B_s \rightarrow D_s^{*+}D_s^{*-}$*
 370 *decays: P wave dilution, penguin and rescattering effects*, Phys. Lett. **B458** (1999)
 371 375, arXiv:hep-ph/9904360.
- 372 [10] A. Datta and D. London, *Extracting γ from $B_d^0(t) \rightarrow D^{(*)+}D^{(*)-}$ and $B_d^0 \rightarrow$*
 373 *$D_s^{(*)+}D_s^{(*)-}$ decays*, Phys. Lett. **B584** (2004) 81, arXiv:hep-ph/0310252.
- 374 [11] R. Fleischer, *Exploring CP violation and penguin effects through $B_d^0 \rightarrow D^+D^-$ and*
 375 *$B_s^0 \rightarrow D_s^+D_s^-$* , Eur. Phys. J. **C51** (2007) 849, arXiv:0705.4421.
- 376 [12] K. De Bruyn *et al.*, *Branching ratio measurements of B_s decays*, Phys. Rev. **D86**
 377 (2012) 014027, arXiv:1204.1735.
- 378 [13] R. Fleischer and R. Knegjens, *Effective lifetimes of B_s decays and their constraints*
 379 *on the B_s^0 - \bar{B}_s^0 mixing parameters*, Eur. Phys. J. **C71** (2011) 1789, arXiv:1109.5115.

- 380 [14] Y. Amhis *et al.*, *Averages of b-hadron, c-hadron, and tau-lepton proper-*
381 *ties as of early 2012*, [arXiv:1207.1158](#), More information is available at
382 www.slac.stanford.edu/xorg/hfag.
- 383 [15] LHCb collaboration, R. Aaij *et al.*, *Measurement of the effective $B_s^0 \rightarrow K^+ K^-$ lifetime*,
384 *Phys. Lett.* **B716** (2012) 393, [arXiv:1207.5993](#).
- 385 [16] LHCb collaboration, R. Aaij *et al.*, *Measurement of the B_s^0 effective lifetime in the*
386 *$J/\psi f_0(980)$ final state*, *Phys. Rev. Lett.* **109** (2012) 152002, [arXiv:1207.0878](#).
- 387 [17] M. Gronau, D. London, and J. Rosner, *Rescattering contributions to rare B meson*
388 *decays*, [arXiv:1211.5785](#).
- 389 [18] Particle Data Group, J. Beringer *et al.*, *Review of particle physics (RPP)*, *Phys. Rev.*
390 **D86** (2012) 010001.
- 391 [19] LHCb collaboration, R. Aaij *et al.*, *Measurement of b-hadron branching frac-*
392 *tions for two-body decays into charmless charged hadrons*, *JHEP* **10** (2012) 037,
393 [arXiv:1206.2794](#).
- 394 [20] Y. Li, C.-D. Lu, and Z.-J. Xiao, *Rare decays $B^0 \rightarrow D_s^{(*)+} D_s^{(*)-}$ and $B_s^0 \rightarrow D^{(*)+} D^{(*)-}$*
395 *in perturbative QCD approach*, *J. Phys.* **G31** (2005) 273, [arXiv:hep-ph/0308243](#).
- 396 [21] J. Eeg, S. Fajfer, and A. Hiorth, *On the color suppressed decay modes $\bar{B}^0 \rightarrow D_s^+ D_s^-$*
397 *and $\bar{B}_s^0 \rightarrow D^+ D^-$* , *Phys. Lett.* **B570** (2003) 46, [arXiv:hep-ph/0304112](#).
- 398 [22] LHCb collaboration, A. A. Alves Jr. *et al.*, *The LHCb detector at the LHC*, *JINST* **3**
399 (2008) S08005.
- 400 [23] M. Adinolfi *et al.*, *Performance of the LHCb RICH detector at the LHC*,
401 [arXiv:1211.6759](#), (submitted to *Eur. Phys. J. C*).
- 402 [24] R. Aaij *et al.*, *The LHCb trigger and its performance*, [arXiv:1211.3055](#), (submitted
403 to *JINST*).
- 404 [25] V. V. Gligorov and M. Williams, *Efficient, reliable and fast high-level triggering using*
405 *a bonsai boosted decision tree*, [arXiv:1210.6861](#), (submitted to *JINST*).
- 406 [26] T. Sjöstrand, S. Mrenna, and P. Z. Skands, *PYTHIA 6.4 Physics and manual*, *JHEP*
407 **05** (2006) 026, [arXiv:hep-ph/0603175](#).
- 408 [27] I. Belyaev *et al.*, *Handling of the generation of primary events in GAUSS, the LHCb*
409 *simulation framework*, *Nuclear Science Symposium Conference Record (NSS/MIC)*
410 **IEEE** (2010) 1155.
- 411 [28] D. J. Lange, *The EvtGen particle decay simulation package*, *Nucl. Instrum. Meth.*
412 **A462** (2001) 152.

- 413 [29] P. Golonka and Z. Was, *PHOTOS Monte Carlo: a precision tool for QED corrections*
414 *in Z and W decays*, Eur. Phys. J. **C45** (2006) 97, [arXiv:hep-ph/0506026](#).
- 415 [30] GEANT4 collaboration, J. Allison *et al.*, *Geant4 developments and applications*,
416 IEEE Trans. Nucl. Sci. **53** (2006) 270; GEANT4 collaboration, S. Agostinelli *et al.*,
417 *GEANT4: A simulation toolkit*, Nucl. Instrum. Meth. **A506** (2003) 250.
- 418 [31] M. Clemencic *et al.*, *The LHCb simulation application, GAUSS: design, evolution and*
419 *experience*, J. of Phys. : Conf. Ser. **331** (2011) 032023.
- 420 [32] I. Narsky, *Optimization of signal significance by bagging decision trees*,
421 [arXiv:physics/0507157](#).
- 422 [33] I. Narsky, *StatPatternRecognition: a C++ package for statistical analysis of high*
423 *energy physics data*, [arXiv:physics/0507143](#).
- 424 [34] M. Pivk and F. R. Le Diberder, *sPlot: a statistical tool to unfold data distributions*,
425 Nucl. Instrum. Meth. **A555** (2005) 356, [arXiv:physics/0402083](#).
- 426 [35] T. Skwarnicki, *A study of the radiative cascade transitions between the Upsilon-prime*
427 *and Upsilon resonances*, PhD thesis, Institute of Nuclear Physics, Krakow, 1986,
428 DESY-F31-86-02.
- 429 [36] Belle Collaboration, A. Drutskoy *et al.*, *Observation of $B \rightarrow D^{(*)}K^-K^{0(*)}$ decays*,
430 Phys. Lett. **B542** (2002) 171, [arXiv:hep-ex/0207041](#).
- 431 [37] LHCb collaboration, R. Aaij *et al.*, *Measurement of the ratio of fragmentation fractions*
432 *f_s/f_d and dependence on B meson kinematics*, [arXiv:1301.5286](#), (submitted to
433 JHEP).
- 434 [38] A. Lenz and U. Nierste, *Numerical updates of lifetimes and mixing parameters of*
435 *B mesons*, [arXiv:1102.4274](#), proceedings of the 6th International Workshop in the
436 CKM Unitarity Triangle, Warwick, U.K., Sept. 6-10, 2010.
- 437 [39] LHCb collaboration, *Tagged time-dependent angular analysis of $B_s^0 \rightarrow J/\psi \phi$ decays*
438 *at LHCb*, LHCb-CONF-2012-002.
- 439 [40] Belle collaboration, S. Esen *et al.*, *Precise measurement of the branching fractions*
440 *for $B_s \rightarrow D_s^{(*)+}D_s^{(*)-}$ and first measurement of the $D_s^{*+}D_s^{*-}$ polarization using e^+e^-*
441 *collisions*, [arXiv:1208.0323](#).
- 442 [41] J. A. Bailey *et al.*, *$B_s \rightarrow D_s/B \rightarrow D$ semileptonic form-factor ratios and their*
443 *application to $\mathcal{B}(B_s^0 \rightarrow \mu^+\mu^-)$* , Phys. Rev. **D85** (2012) 114502, [arXiv:1202.6346](#).